CHAPTER 1

Microunit Operations and Continuous Flow Chemical Processing

Arata Aota[1] and **Takehiko Kitamori**[2,*]

Contents

Abstract

Integrated microchemical systems on microchips are expected to become important tools for analysis and synthesis within the biological sciences and technologies. For these purposes, general integration concepts were developed, including microunit

1 Institute of Microchemical Technology, and Micro Chemistry Group, Kanagawa Academy of Science and Technology, 3-2-1 Sakado, Takatsu, Kawasaki, Kanagawa 213-0012, Japan

2 Department of Applied Chemistry, School of Engineering, The University of Tokyo, 7-3-1 Hongo, Bunkyo, Tokyo 113-8656, Japan, and Micro Chemistry Group, Kanagawa Academy of Science and Technology, 3-2-1 Sakado, Takatsu, Kawasaki, Kanagawa 213-0012, Japan

* Corresponding author.
E-mail address: mailto:kitamori@icl.t.u-tokyo.ac.jp

Advances in Chemical Engineering, Volume 38
ISSN: 0065-2377, DOI 10.1016/S0065-2377(10)38001-X

operations and continuous-flow chemical processing. The general methodology has enabled analysis, synthesis, and construction of biochemical systems on microchips, and these microsystems have demonstrated superior performance (i.e., rapid, simple, and highly efficient processing). Microchemical technology has now entered the phase of practical application. In this chapter, we discuss general methods, and applications of microchemical systems on microchips.

1. INTRODUCTION

Integrated microchemical systems are essential tools for high-speed, functional, and compact instrumentations used for analysis and synthesis, biological sciences, and technologies. In the 1990s, most microchip-based systems were used for gene or protein analysis and employed electrophoretic separation with laser-induced fluorescence detection (Auroux et al., 2002; Reyes et al., 2002). However, other analytical and synthesis methods were required for more general analytical, combinatorial, physical, and biochemical applications that involve complicated chemical processes, organic solvents, neutral species, and nonfluorescent molecule detection. For these applications, general microintegration methods on microchips became quite important.

General methods for microintegration of chemical systems that are similar to systems used in electronics have been developed (Figure 1). Instead of the resistor, capacitor, and diode, mixing, extraction, phase separation, and other unit operations of chemical processes are integrated as components. These unit operations are known as microunit operations (MUOs), and like the parts of an electric circuit. They can combine with one another in parallel and in serial by continuous-flow chemical processing (CFCP). The function of the microchemical chip is analogous to that of a chemical central processing unit. In order to realize these basic concepts, fluidic control methods are quite important, and parallel multiphase microflows were realized by partial surface modification and channel structures which enabled various MUOs and flexible integration of the MUOs connected by CFCP. This technique has demonstrated superior performance in shorter processing times (from days or hours to minutes or seconds), smaller sample and reagent volumes (down to a single drop of blood), easier operation (from professional to personal), and smaller system sizes (from 10 m chemical plants to desktop plants to mobile systems) compared to conventional analysis, diagnosis, and chemical synthesis systems. Practical prototype systems have also been realized in environmental analysis, clinical diagnosis, cell analysis, gas analysis, medicine synthesis, microparticle synthesis, and so on. For example, a

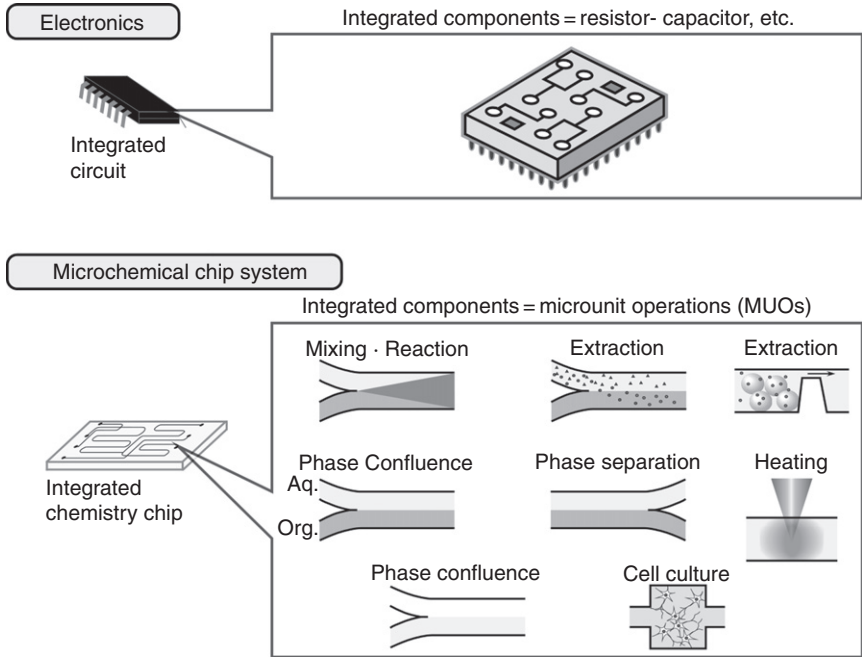

Figure 1 A microchemical chip system compared with an electronic system.

portable microELISA (enzyme-linked immunosorbent assay) system was recently constructed where the analysis time was several minutes, rather than several hours as in the conventional technique. The sample volume (5 μl) was also considerably smaller than the volume (several milliliters) required for conventional diagnosis. In addition, the operation itself was much easier, and its correlation with conventional methods was confirmed with real blood samples. These features are promising for point-of-care (POC) clinical diagnosis.

Microtechnology is moving in two directions. The first is the practical application. Although some practical prototype systems have been realized, attaining long-term stability in parallel liquid/liquid and liquid/gas microflows can be sometimes problematic, and the interfaces are distorted. For robust fluidic control, methods for stabilizing or recovering parallel multiphase microflows are essential. For microfluidic devices, the ability to process small (nanoliter to microliter volume) samples and to interface with microchips is important. In addition, smart fluidic devices (valves or pumps) for flexible and reliable liquid handling on microchips are required for more complex and high-throughput chemical processing on microchip.

The second direction involves new science in nanoscale (10–1,000 nm) space, called as extended nanospace. The extended nanospace is an important region in bridging the gap between single molecules and the condensed phase. Recently, general methodologies in microspace were applied to extended nanospace demonstrating that the basic methodologies in microspace are applicable to extended nanospace. Water displays remarkably different properties in the extended nanospace channel. A model fundamentally related to the surface chemistry of the nanochannel was proposed. This model was applied to protein analysis of a countable number of molecules, and the same type of integrated approach (extended nanospace channels embedded in microfluidic systems) was applied to control and analysis of cell immobilization and culture.

Here, we introduce these basic methodolodgies and applications. Firstly, the general concepts (MUO and CFCP) for microintegration in Chapter 2, and fluid control methods to support the MUO and CFCP in Chapter 3 are discussed.

2. DESIGN AND CONSTRUCTION METHODOLOGY FOR INTEGRATION OF MICROCHEMICAL SYSTEMS

Integrated microchemical systems are expected to be applied in various fields. In order to realize general analytical, combinatorial, physical, and biological applications, general microintegration methods on microchips are quite important. Conventional macroscale chemical plants or analytical systems are constructed combining unit operations such as mixer, reactors, and separators. Similar methodology can be applied to the microchemical systems. By combining MUOs with different functions in series and in parallel, various chemical processes can be integrated into microchips through use of a multiphase microflow network such as that shown in Figure 2. This methodology is termed CFCP (Tokeshi et al., 2002). Miniaturizing conventional unit operations is often not effective and sometimes does not work at all, because many physical properties (e.g., heat and mass transfer efficiency, specific interfacial area, and vanishingly small gravity force) are significantly different in microspace. Therefore, novel MUOs taking these issues into account are needed. Kitamori and colleagues have developed MUOs for various purposes, such as mixing and reaction (Sato et al., 1999; Sorouraddin et al., 2000, 2001), phase confluence and separation (Aota et al., 2007a, 2007b; Hibara et al., 2002, 2003; Hisamoto et al., 2001a, 2001b, 2003; Hotokezaka et al., 2005; Kikutani et al., 2004; Minagawa et al., 2001; Miyaguchi et al., 2006; Sato et al., 2000b; Smirnova et al., 2006, 2007; Surmeian et al., 2001, 2002; Tokeshi et al., 2000a, 2000b), solvent extraction (Aota et al., 2007a, 2007b; Hibara et al., 2001, 2003; Hisamoto et al., 2001a, 2001b; Hotokezaka

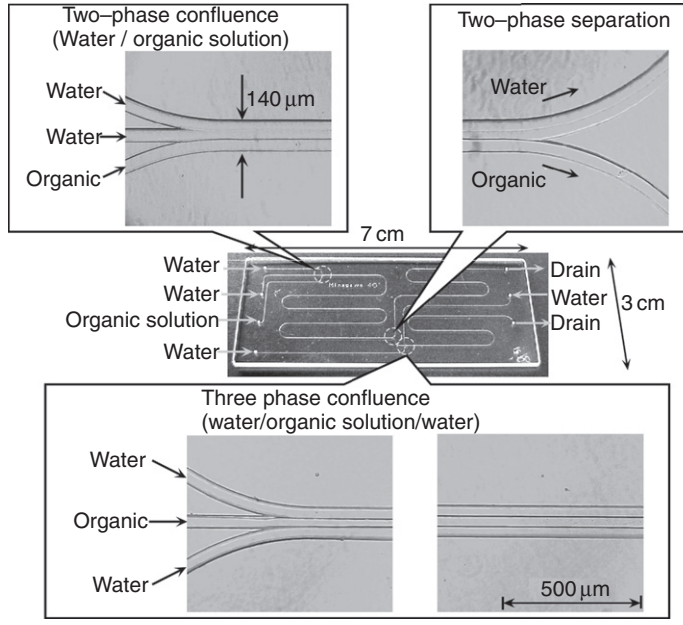

Figure 2 Multiphase microflow network (Tokeshi et al., 2002).

et al., 2005; Kikutani et al., 2004; Minagawa et al., 2001; Miyaguchi et al., 2006; Sato et al., 2000b; Smirnova et al., 2006, 2007; Surmeian et al., 2001, 2002; Tokeshi et al., 2000a, 2000b, 2002), gas–liquid extraction (Aota et al., 2009b; Hachiya et al., 2004), solid-phase extraction and reaction on surfaces (Kakuta et al., 2006; Ohashi et al., 2006; Sato et al., 2000a, 2001, 2003, 2004), heating (Goto et al., 2005; Slyadnev et al., 2001; Tanaka et al., 2000), cell culture (Goto et al., 2008; Tamaki et al., 2002; Tanaka et al., 2004, 2006), and ultrasensitive detection (Hiki et al., 2006; Mawatari et al., 2006; Proskurnin et al., 2003; Tamaki et al., 2002, 2003, 2005; Tokeshi et al., 2001, 2005; Yamauchi et al., 2006) (Figure 3).

2.1 Multiphase microflow network

For many chemical processing applications, microchemical systems should include solvent extraction and interfacial reaction components utilizing both aqueous and organic (or gas and liquid) solutions. Both solutions must be controlled to realize general chemistry in a microchip. In 1990s, electroosmotic flow was used in microchip electrophoresis (Auroux et al., 2002; Reyes et al., 2002); however, the electroosmotic flow is restricted to the flow control of only one type solution (aqueous buffer). Therefore, electroosmotic flow is not suitable for a flow-control method to

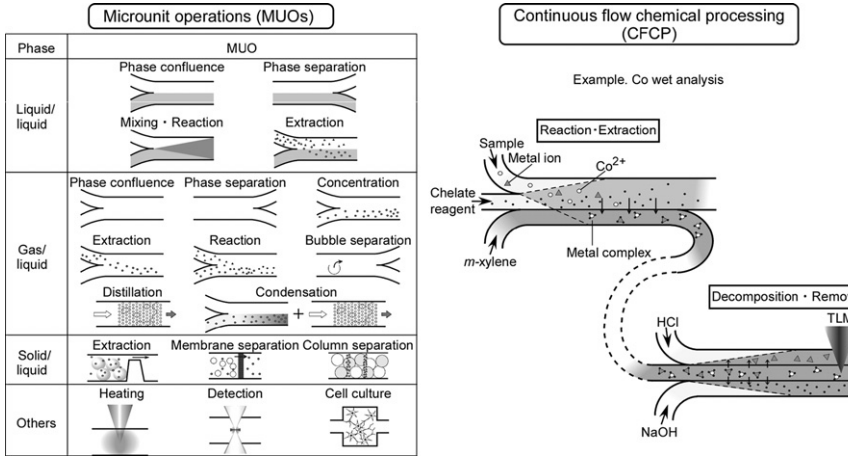

Figure 3 MUOs and CFCP. Abbreviation: TLM, thermal lens microscope (Tokeshi et al., 2002).

integrate various chemical processes that require other types of solvents. Simple pressure-driven flow has been used by many researchers as a nonelectrical pumping method (Brody and Yager, 1997; Kopp et al., 1998; Weigl and Yager, 1999).

Recently, microsegmented flows of immiscible solutions were used for microchemical processes (Burns and Ramshaw, 2001; Kralj et al., 2005; Sahoo et al., 2007; Song et al., 2003). Although the microsegmented flows are advantageous in mixing and rapid molecular transport, phase separation and more than three-phase contact are difficult. Furthermore, controlling the microsegmented flows in the wide range of the flow rates is difficult because the size of the segments changes along with the flow rate ratio. Kitamori et al. have developed parallel multiphase microflows, which flow side-by-side along the microchannels (Hibara et al., 2001). Parallel multiphase microflows in laminar flow regime allow better design and control of microchemical processes because the parallel multiphase microflows are stable in a wide range of the flow rates and can create more than three-phase contact.

2.2 Example of microchemical processes

2.2.1 Molecular transport in microspace

Microfluidic chemical processes are based on transverse molecular diffusion to the microchannel. In microspace, because the diffusion distance is short, rapid chemical processes are expected there. In order to clarify the time required for chemical processes in microspace, diffusion time t in one

dimension is considered for a simple discussion. t in one dimension is characterized as follows:

$$t = \frac{l_d^2}{K} \tag{1}$$

where l_d and K are the diffusion length and the diffusion coefficient. Figure 4 shows the diffusion time dependence on the diffusion length. Solid and dashed lines correspond to the diffusion time when the respective diffusion coefficients are 1×10^{-9} and $1 \times 10^{-10}\,m^2\,s^{-1}$. In 100-μm-wide microchannels, diffusion time is just 10 s for a sample having a diffusion coefficient of $1 \times 10^{-9}\,m^2\,s^{-1}$. Therefore, samples of high diffusion coefficients, for example, metal chelates, are rapidly transported in microspace. However, diffusion time is 100 s for a sample having a diffusion coefficient of samples of $1 \times 10^{-10}\,m^2\,s^{-1}$. Samples of low diffusion coefficient, for example, DNA and proteins, cannot be quickly transported in microspace.

2.2.2 Co wet analysis

Micro cobalt wet analysis is an example of CFCP that has been demonstrated (Figure 5) (Tokeshi et al., 2002). Conventional procedures for such analysis consist of a chelating reaction, a solvent extraction of the complex, and a decomposition and removal of coexisting metal complex. These procedures are analogous to the conventional unit operations; mixing and reaction, phase confluence, solvent extraction, phase separation, phase confluence, and solvent extraction. These unit operations, in the same way, are analogous to the MUOs. CFCP is designed by combining the MUOs in series and in parallel, as shown in Figure 3.

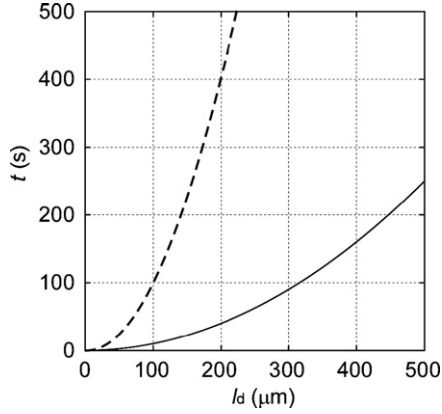

Figure 4 Diffusion time dependence on the diffusion length. Solid and dashed lines correspond to the diffusion time when the respective diffusion coefficients are 1×10^{-9} and $1 \times 10^{-10}\,m^2\,s^{-1}$.

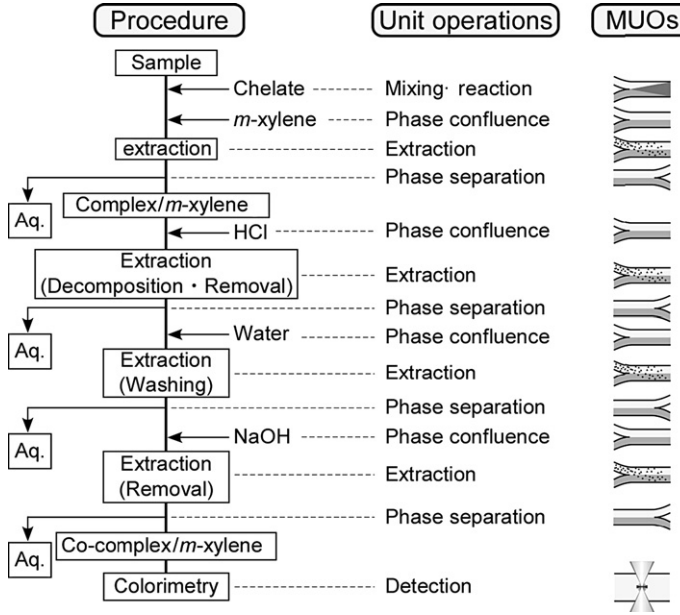

Figure 5 Designing of Co wet analysis systems based on CFCP.

The microchip consists of two different areas, one for reaction and extraction and the other for purification (i.e., decomposition, extraction, and removing impure chelates). In the reaction area, the sample solution containing Co(II), 2-nitroso-1-naphthol (NN), and *m*-xylene were introduced at a constant flow rate through three inlets using microsyringe pumps. These three flows converge at the intersection point, and parallel two-phase microflows, consisting of an organic–aqueous interface, forms in the microchannel. The chelating reaction of Co(II) and NN, and extraction of the Co–NN chelates proceed as the reacting mixture flows along the microchannel. Because NN reacts with coexisting metal ions, such as Co (II), Ni(II), and Fe(II), these coexisting metal chelates are also extracted into the *m*-xylene microflow. Therefore, purification is needed after extraction.

The coexisting metal chelates are decomposed when they make contact at the HCl–*m*-xylene interface, and the metal ions are dissolved in the HCl solution phase. The decomposed fragment of NN is dissolved in NaOH solution, and the Co–NN chelate is stable in concentrated HCl and NaOH solutions, where it remains. Finally, the target chelates in *m*-xylene are detected by a thermal lens microscope downstream, where the Co(II) in aqueous solutions was successfully determined. The limit of detection (2σ) was 0.13 zmol or 78 chelate molecules. The analysis time in this system is only 50 s versus 6 h for conventional devices. Micro chemical processing through use of CFCP has been demonstrated on numerous occasions (Table 1).

Table 1 Example of microchemical processing

Method	Analyte	Limit of detection	Analysis time	Reference
Solvent extraction	Iron complex	7.7 zmol	60 s	Tokeshi et al. (2000)
	Cobalt complex	0.13 zmol, 0.72 zmol, 0.072 zmol	60 s, 50 s, 0 min	Tokeshi et al. (2000, 2002), Minagawa et al. (2001)
	Nickel complex	NA	5 min	Sato et al. (2000)
	K^+ and Na^+	4.5 zmol	1 s	Hisamoto et al. (2001a, 2001b)
	Dye molecules	NA, NA	6 s, 4 s	Surmeian et al. (2001, 2002)
	Amphetamines	0.5 μg ml^{-1}	15 min	Miyaguchi et al. (2006)
	Carbaryl	0.5 zmol, 0.079 zmol	4.5 min, 5 min	Smirnova et al. (2006, 2007)
	Uran (VI)	0.86 amol	1 s	Hotokezaka et al. (2005)
Gas extraction	Formaldehyde	8.9 ppb	30 min	Hachiya et al. (2004)
	Ammonia	1.4 ppb	16 min	Aota et al. (2009b)
Immunoassay	S-IgA	<1 μg ml^{-1}	<1 h	Sato et al. (2000)
	Carcinoembryonic antigen	30 pg ml^{-1}	35 min	Sato et al. (2001)
	Interferon-γ	10 pg ml^{-1}	50 min (four samples)	Sato et al. (2003)

Table 1 *(Continued)*

Method	Analyte	Limit of detection	Analysis time	Reference
	B-type natriuretic peptide	0.1 pg ml^{-1}	35 min	Sato et al. (2004)
	IgE	2 ng ml^{-1}	12 min	Kakuta et al. (2006)
	Prion	50 pg ml^{-1}	15 min	–
	C-reactive protein	20 ng ml^{-1}	8 min	–
	Amphetamines	0.1 ng ml^{-1}	10 min	–
Flow Injection	Fe^{2+}	6 zmol	150 s	Sato et al. (1999)
	Ascorbic acid	1 zmol	30 s	Sorouraddin et al. (2000)
	Catecholamines	2 zmol	15 s	Sorouraddin et al. (2001)
Enzymatic assay	H_2O_2	NA, 50 zmol, NA	250 s, NA, NA	Hisamoto et al. (2003), Tanaka et al. (2000, 2004)

The CFCP approach can be applied to develop more complicated processing system. More rapid analysis, bioassays, and immunoassays, as well as more efficient reaction and extraction, can be achieved through CFCP systems as compared to conventional devices. However, development of complicated microchemical processing systems is time consuming because of the need to determine appropriate conditions for each reaction and separation process at the miniaturized scale, and also design and optimize the microchannel structure. In semiconductor circuit device design, computer-aided design (CAD) is typically used to perform circuit analysis, integrated device analysis, layout design, and logical simulation. If CAD is developed specifically for microchemical processing, which includes microfluid simulation, reaction time analysis, extraction time analysis, and microchannel structure design, the time of development for these systems would be drastically shortened.

2.2.3 Microimmunoassay

Immunoassay is one of the most important analytical methods for clinical diagnosis. Heterogeneous immunoassay is a particularly popular approach, wherein captured antibodies or antigens fixed on a solid surface react with serum target antigens or antibodies. Labeled secondary antibodies then capture the targets, and the target amounts are quantified by detecting the labels. Heterogeneous immunoassay features easy and accurate bound-free separation, which is important for improving limit of detection (LOD). Shortening analysis time is necessary when dealing with smaller samples and reagent volumes, given increasing demand in POC diagnosis. In conventional methods, a microtiter plate well (typically 0.65 mm in diameter) is used, and the specific interfacial area for 50 μl volumes is 13 cm^{-1}. However, when a microchannel (200 μm deep and 200 μm wide) is utilized for immobilizing the antibodies (antigens), the interfacial area, which affects the reaction time and efficiency, increases to 200 cm^{-1}.

Kitamori et al. have reported the first successful integration of ELISA into a microchip (Kakuta et al., 2006; Sato et al., 2000a, 2001, 2003, 2004). They developed a new MUO for the heterogeneous reaction through the use of bead-packed microchannels (Figure 6). They immobilized antibodies (antigens) on the bead surface via physisorption or chemisorption. After immobilization, the authors applied a bovine serum albumin or MPC (2-methylacryloyloxyethyl phosphorylcholone) polymer coating to minimize nonspecific adsorption. A microbead suspension with captured antibodies was introduced and stopped at a microchannel dam structure (with a 10 μm gap), and a 5–10-mm-long area of packed beads area was formed. The target sample solution was introduced and captured by the antibodies (antigens). Enzyme-conjugated secondary (horseradish peroxidase (HRP) or alkaline phosphatase (ALP)) antibodies were then introduced to capture the antigens. Finally, substrates were applied, and the dye molecules

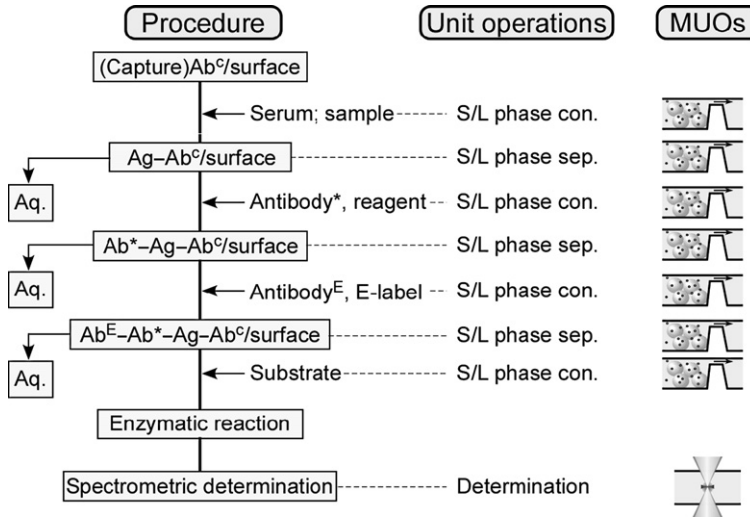

Figure 6 Designing of microimmunoassay.

produced by the enzymatic reaction were detected by thermal lens microscope (TLM), downstream from the microbeads.

Instrumentation for easy operation and high precision is also an important for clinical diagnostic systems. Usually, fluidic handling in microchannels is complex and difficult due to the lack of low volume (1 μl) valves or fluidic interfaces from macroscale to microscale without generating dead volume of microliter scale. Furthermore, it is advisable that microchips be replaced when new measurements are taken, or laborious procedures to remove antigens and wash the microchannels are required. These factors limit the expansion of microchip technologies for clinical diagnosis. The developed method features the utilization of microbeads for immunoreactions; and by simply introducing new microbeads, new measurements can easily be taken. Recently, Kitamori et al. developed a portable micro-ELISA system for POC clinical diagnosis by designing a simple microfluidic system with integrated fluidics, optics, and electronics (Ohashi et al., 2006). An example of our system and the components for four parallel measurements are illustrated in Figure 7. The samples and reagents are stocked in tubes on a moving tray. A PEEK™ tube, under the control of four syringe pumps, aspirates and injects the samples and reagents (microliter volume) into the microchip. The diversion of flow, to either waste or microchip, is controlled by their novel, low volume (~1 μl) and fast response time (<1 s), microvalve. The tube is connected to the microchip through a hydrophobic connector with pressure resistance of >1 MPa. Under a maximal flow rate of 10 μl min^{-1} during washing process, the pressure drop at the bead-packed area is <100 kPa. Immunoassay is then conducted on the microchip and detected

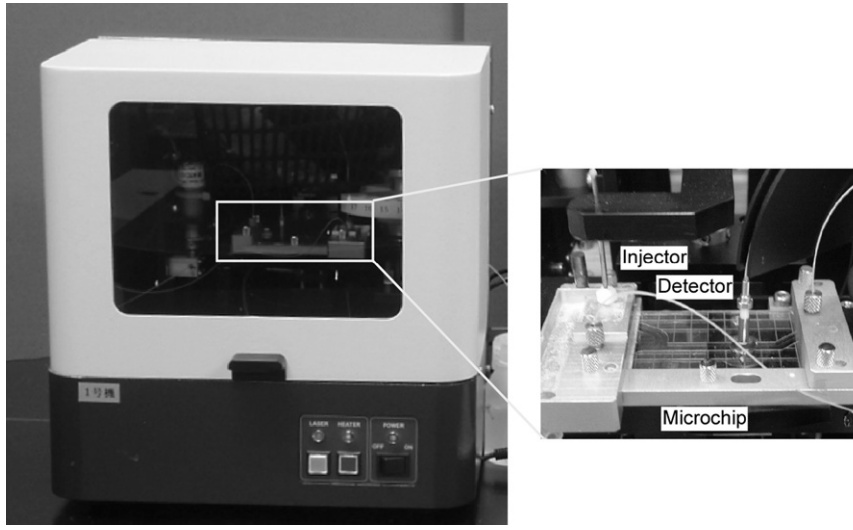

Figure 7 Picture of a micro-ELISA system (Ohashi et al., 2006).

by an on-chip TLM (Tokeshi et al., 2005). In this case, stopped-flow conditions were utilized for the enzymatic reaction, and signals were obtained as a clear peak for each channel. All the processes are controlled by software on a PC.

2.2.4 Stimulant analysis in urine

Urine analysis for illegal drugs is increasingly performed in forensic laboratories (especially in Japan). Gas chromatography–mass spectrometry (GC–MS) is extensively used because of its versatility and reliability. By way of sample preparation for GC analysis, conventional liquid–liquid extraction has a widespread use, but it is not only laborious but also environmentally unfriendly due to the consumption of considerable amounts of organic solvents. Therefore, microintegration of the sample preparation procedure is required.

Conventional procedures and corresponding MUOs are illustrated in Figure 8 (Miyaguchi et al., 2006). Urine samples are mixed with organic solvent (1-Chlorobutane) and stimulants in urine are extracted. After phase separation, the organic solution is mixed with derivatization reagent (trifluoroacetic anhydride). Unreacted derivatization reagents were washed by extracting with water. The washed organic solution was collected in a vial, and the concentration was determined by GC–MS. These conventional processes are easily dissolved to unit operations and converted to corresponding MUOs. The MUOs can be integrated to microchips by CFCP as shown in Figure 9. The conventional procedures can be simplified by the multiphase microflow network. The sample preparation time was decreased from several

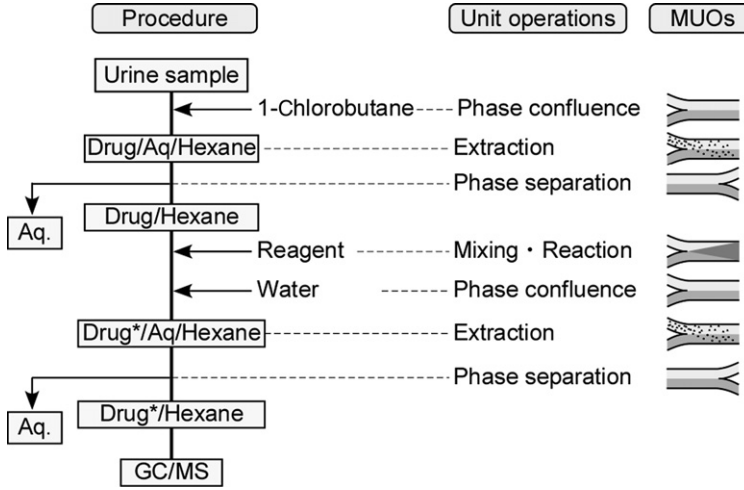

Figure 8 Designing of urine analysis systems based on MUOs and CFCP.

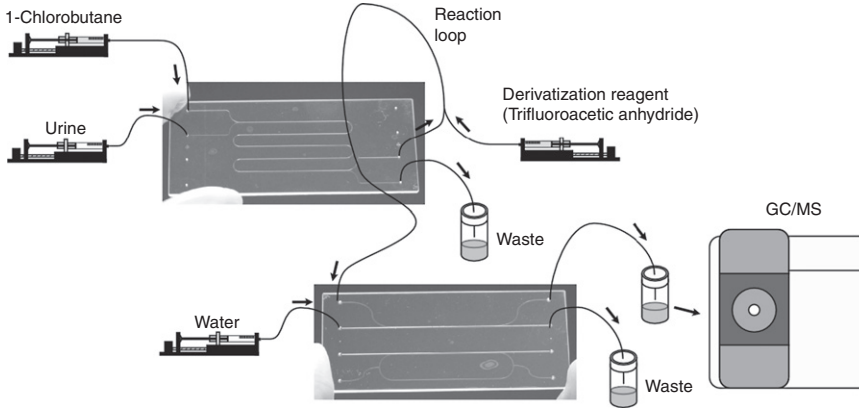

Figure 9 Microsystems for urine analysis (Miyaguchi et al., 2006).

hours to 5 min, and total analysis time including GC–MS is below 20 min. In addition, just 100 μl of sample and reagent are required. These features will open on-site and precise urine analysis in near future.

3. SURFACE CHEMISTRY FOR MULTIPHASE MICROFLOWS

3.1 Fundamental physical properties of multiphase microflows

Control of multiphase microflows is an important basic technology for integration of MUOs. Therefore, control methods for the stable phase separation of the multiphase microflows in a wide range of the flow

rates are required. However, the methods in the conventional size devices cannot be applied because the physical properties in the microspace are different from those in macrospace. In conventional devices, the aqueous and organic phases are separated by gravity. In the microspace, however, the fluid is greatly influenced by liquid–solid, liquid–gas, and liquid–liquid interfaces because of the large specific interfacial area. To clarify the main physical forces in the microchannels which include viscous force and interfacial parameter and can be analyzed using the dimensionless Reynolds (Re) and Bond (Bo) numbers, defined as an inertia-to-viscous force ratio and a gravity-to-tension ratio, respectively. Figure 10a shows a cross section of a model microchannel with dimensions included in these parameters.

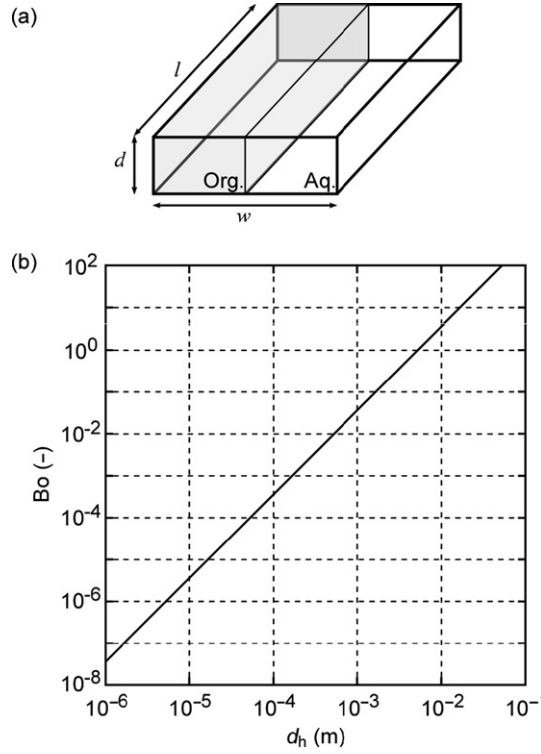

Figure 10 (a) The liquid–liquid interface between the aqueous an organic phases (Aq. and Org.) in a model microchannel. The width, depth, and length along the microchannel are represented as *w*, *d*, and *l*, respectively. (b) Bond number (Bo) dependence on the hydrodynamic diameter for water–toluene microflows.

Bo is defined as

$$\mathrm{Bo} = \frac{(\Delta\rho) g d_\mathrm{h}^2}{\gamma} \tag{2}$$

where $\Delta\rho$, γ, and d_h are the density difference, the interfacial tension between the two phases, and equivalent diameter, respectively, and where g is the gravitational acceleration ($9.8\,\mathrm{m\,s^{-2}}$). The variable d_h corresponds to the mean hydraulic diameter defined as

$$d_\mathrm{h} = \frac{4S}{l_\mathrm{p}} \tag{3}$$

where S is the cross section and l_p is the perimeter of a section of the microchannel. Figure 10b shows the Bo of the water–toluene two phase flows as a function of the d_h ($\Delta\rho = 0.132 \times 10^3\,\mathrm{kg\,m^{-3}}$, $\gamma = 36.3\,\mathrm{mN\,m^{-1}}$). In microspace with a d_h of 100 μm, the interfacial tension exceed gravity by three orders of magnitude.

Re is defined as

$$\begin{aligned} \mathrm{Re} &= \frac{\rho u d_\mathrm{h}}{\mu} \\ &= \frac{2\rho u d w}{\mu(w + 2d)} \end{aligned} \tag{4}$$

where ρ, u, and μ are the density, the mean velocity, and the viscosity, respectively. When water flows in the microchannel at the flow rate of $1\,\mu\mathrm{l\,min^{-1}}$, Re becomes only 0.05 in microspace with a d_h of 100 μm. Therefore, multiphase microflows are considered as laminar flow.

When physical and properties of the multiphase microflows such as viscosity and interfacial tension can be regarded as constant, the flow can be divided in two parts. One is a transient part where the flow profile is gradually approaching an equilibrium state after confluence, and the other is an equilibrium part. The flow vector profile of the latter can be expressed analytically with simple assumptions. At first, two-phase microflows in the equilibrium state is considered. The two-phase microflows are illustrated in Figure 11. Phase I and II have viscosities of μ^I and μ^II and widths of a and b, respectively. As driving force of the flow, pressure difference of $P_\mathrm{L} - P_0 \equiv \Delta P$ is assumed for a channel length of L. The x- and z-axes are defined as directions across and along the channel, respectively. The origin of the x-axis is assumed at the interface of phases I and II. Under these conditions, shear stress τ_{xz} can be expressed based on momentum balance as

$$\frac{\mathrm{d}\tau_{xz}}{\mathrm{d}x} = \frac{\Delta P}{L} \tag{5}$$

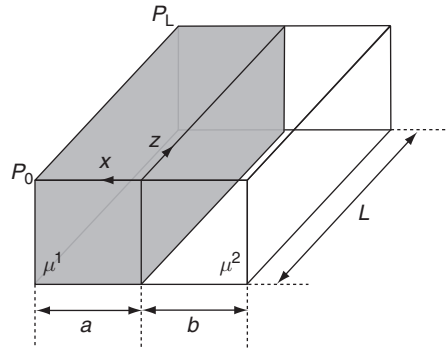

Figure 11 Illustration of two-phase microflows. Phases I and II have viscosities of μ^{I} and μ^{II}, and widths of *a* and *b*, respectively.

In order to obtain the stress for phases I and II, integral calculus of Equation (4) is expressed as

$$\begin{aligned} \tau_{xz}^{\mathrm{I}} &= \frac{\Delta P}{L}x + C_1^{\mathrm{I}} \\ \tau_{xz}^{\mathrm{II}} &= \frac{\Delta P}{L}x + C_1^{\mathrm{II}} \end{aligned} \tag{6}$$

where C_1 is constant and superscripts I and II mean phases I and II. Here, continuity of shear stress is assumed as a boundary condition. Namely,

$$\tau_{xz}^{\mathrm{I}} = \tau_{xz}^{\mathrm{II}} \text{ at } x = 0 \tag{7}$$

By substituting Equation (6) with Equation (7), the following relationship is obtained.

$$C_1^{\mathrm{I}} = C_1^{\mathrm{II}} = C_1 \tag{8}$$

Here, Newton's law of viscosity is used,

$$\tau_{xz} = \mu \frac{\mathrm{d}v_z}{\mathrm{d}x} \tau_{xz}^{\mathrm{II}} \tag{9}$$

where v_z is flow velocity in the *z*-direction. By using Equations (6)–(9), the velocities of phases I and II, v^{I} and v^{II}, are expressed as

$$\begin{aligned} v_z^{\mathrm{I}} &= \frac{\Delta P}{2L\mu^{\mathrm{I}}}x^2 + \frac{C_1}{\mu^{\mathrm{I}}}x + C_2^{\mathrm{I}} \\ v_z^{\mathrm{II}} &= \frac{\Delta P}{2L\mu^{\mathrm{II}}}x^2 + \frac{C_1}{\mu^{\mathrm{II}}}x + C_2^{\mathrm{II}} \end{aligned} \tag{10}$$

where C_2 is a constant. Here, consistency of v_z^{I} and v_z^{II} at the interface and nonslip conditions are assumed as boundary conditions. Namely,

$$\begin{aligned} &v_z^{\mathrm{I}} = v_z^{\mathrm{II}} \text{ at } x = 0 \\ &v_z^{\mathrm{I}} = 0 \text{ at } x = a \\ &v_z^{\mathrm{II}} = 0 \text{ at } x = -b \end{aligned} \tag{11}$$

From Equations (10) and (11), C_1, ${C_2}^{\mathrm{I}}$, and ${C_2}^{\mathrm{II}}$ are eliminated as

$$v_z^{\mathrm{I}} = \frac{\Delta P}{L}\frac{a^2}{\mu^{\mathrm{I}}}\left[1 + \frac{\frac{b^2}{a^2}\mu^{\mathrm{I}} - \mu^{\mathrm{II}}}{\frac{b}{a}\mu^{\mathrm{I}} + \mu^{\mathrm{II}}} + \frac{\frac{b^2}{a^2}\mu^{\mathrm{I}} - \mu^{\mathrm{II}}}{\frac{b}{a}\mu^{\mathrm{I}} + \mu^{\mathrm{II}}}\left(\frac{x}{a}\right) - \left(\frac{x}{a}\right)^2\right] \tag{12}$$

$$v_z^{\mathrm{II}} = \frac{\Delta P}{L}\frac{b^2}{\mu^{\mathrm{II}}}\left[1 - \frac{\mu^{\mathrm{I}} - \frac{a^2}{b^2}\mu^{\mathrm{II}}}{\mu^{\mathrm{I}} + \frac{b}{a}\mu^{\mathrm{II}}} + \frac{\mu^{\mathrm{I}} - \frac{a^2}{b^2}\mu^{\mathrm{II}}}{\mu^{\mathrm{I}} + \frac{b}{a}\mu^{\mathrm{II}}}\left(\frac{x}{b}\right) - \left(\frac{x}{b}\right)^2\right] \tag{13}$$

From Equations (12) and (13), the flow velocity profile can be calculated. By integrating these equations along the x-direction, average velocities for phases I and II, $\langle {v_z}^{\mathrm{I}} \rangle$ and $\langle {v_z}^{\mathrm{II}} \rangle$, are expressed as

$$\left\langle v_z^{\mathrm{I}} \right\rangle = \frac{1}{a}\int_0^a v_z^{\mathrm{I}}\,\mathrm{d}x = \frac{\Delta P}{12L}\frac{a^2}{\mu^{\mathrm{I}}}\left(4 + \frac{3}{a}\frac{b^2\mu^{\mathrm{I}} - a^2\mu^{\mathrm{II}}}{b\mu^{\mathrm{I}} + a\mu^{\mathrm{II}}}\right) \tag{14}$$

$$\left\langle v_z^{\mathrm{II}} \right\rangle = \frac{1}{b}\int_{-b}^0 v_z^{\mathrm{II}}\,\mathrm{d}x = \frac{\Delta P}{12L}\frac{a^2}{\mu^{\mathrm{II}}}\left(4 - \frac{3}{b}\frac{b^2\mu^{\mathrm{I}} - a^2\mu^{\mathrm{II}}}{b\mu^{\mathrm{I}} + a\mu^{\mathrm{II}}}\right) \tag{15}$$

The volume flow ratio to achieve the width ratio of a/b is expressed as

$$\frac{b\left\langle v_z^{\mathrm{II}} \right\rangle}{a\left\langle v_z^{\mathrm{I}} \right\rangle} = \frac{\mu^{\mathrm{I}}}{\mu^{\mathrm{II}}}\frac{b^3}{a^3}\frac{b^2\mu^{\mathrm{I}} + (4ab + 3a^2)\mu^{\mathrm{II}}}{(3b^2 + 4ab)\mu^{\mathrm{I}} + a^2\mu^{\mathrm{II}}} = \frac{b}{a}\frac{3 + 4\left(\frac{b}{a}\right) + \left(\frac{b}{a}\right)^2\frac{\mu^{\mathrm{I}}}{\mu^{\mathrm{II}}}}{3 + 4\left(\frac{a}{b}\right) + \left(\frac{a}{b}\right)^2\frac{\mu^{\mathrm{II}}}{\mu^{\mathrm{I}}}} \tag{16}$$

When the width of the phase I is equal to that of phase II, $a = b$, the flow velocity can be expressed as

$$v_z^{\mathrm{I}} = \frac{\Delta P}{2L}\frac{a^2}{\mu^{\mathrm{I}}}\left[\frac{2\mu^{\mathrm{I}}}{\mu^{\mathrm{I}} + \mu^{\mathrm{II}}} + \frac{\mu^{\mathrm{I}} - \mu^{\mathrm{II}}}{\mu^{\mathrm{I}} + \mu^{\mathrm{II}}}\left(\frac{x}{a}\right) - \left(\frac{x}{a}\right)^2\right] \tag{17}$$

$$v_z^{\mathrm{II}} = \frac{\Delta P}{2L}\frac{a^2}{\mu^{\mathrm{II}}}\left[\frac{2\mu^{\mathrm{II}}}{\mu^{\mathrm{I}} + \mu^{\mathrm{II}}} + \frac{\mu^{\mathrm{I}} - \mu^{\mathrm{II}}}{\mu^{\mathrm{I}} + \mu^{\mathrm{II}}}\left(\frac{x}{a}\right) - \left(\frac{x}{a}\right)^2\right] \tag{18}$$

In the same way, average velocities for $a = b$ can be expressed as

$$\left\langle v_z^{\mathrm{I}} \right\rangle = \frac{1}{a}\int_0^a v_z^{\mathrm{I}}\,\mathrm{d}x = \frac{\Delta P}{12L}\frac{a^2}{\mu^{\mathrm{I}}}\left(\frac{7\mu^{\mathrm{I}}+\mu^{\mathrm{II}}}{\mu^{\mathrm{I}}+\mu^{\mathrm{II}}}\right) \tag{19}$$

$$\left\langle v_z^{\mathrm{II}} \right\rangle = \frac{1}{b}\int_{-b}^0 v_z^{\mathrm{II}}\,\mathrm{d}x = \frac{\Delta P}{12L}\frac{a^2}{\mu^{\mathrm{II}}}\left(\frac{\mu^{\mathrm{I}}+7\mu^{\mathrm{II}}}{\mu^{\mathrm{I}}+\mu^{\mathrm{II}}}\right) \tag{20}$$

The volume flow ratio to achieve the equal widths is expressed as

$$\frac{b\left\langle v_z^{\mathrm{II}} \right\rangle}{a\left\langle v_z^{\mathrm{I}} \right\rangle} = \frac{\mu^{\mathrm{I}}}{\mu^{\mathrm{II}}}\frac{\mu^{\mathrm{I}}+7\mu^{\mathrm{II}}}{7\mu^{\mathrm{I}}+\mu^{\mathrm{II}}} = \frac{7+\dfrac{\mu^{\mathrm{I}}}{\mu^{\mathrm{II}}}}{7+\dfrac{\mu^{\mathrm{II}}}{\mu^{\mathrm{I}}}} \tag{21}$$

Figure 12 shows flow velocity profiles calculated based on Equations (17) and (18) for the two-phase microflows of water (1.0 cP)/octanol (7.3 cP),

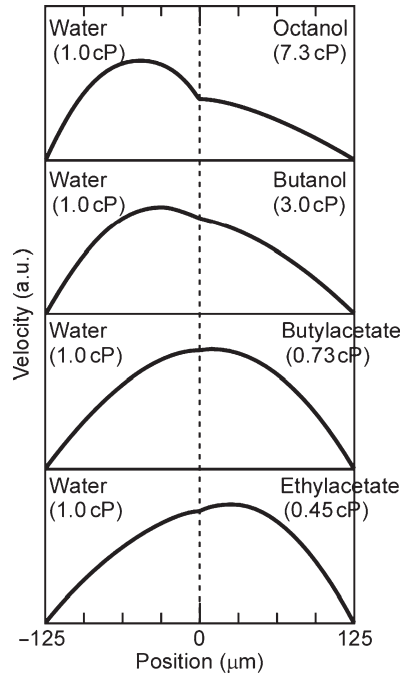

Figure 12 Calculated flow velocity profiles for 4 two-phase microflows with the same pressure. Channel width of 250 μm is assumed.

water/butanol (3.0 cP), water/butyl acetate (0.73 cP), and water/ethyl acetate (0.43 cP).

Multiphase microflows are dominated by pressures (Aota et al., 2007a, 2009a). One important parameter needed to describe the multiphase microflows is the pressure that drives the fluids. The pressure decreases in the downstream part of the flow because of the fluids' viscosity. When two fluids in contact with one another have different viscosities, the pressure difference (ΔP_{Flow}) between the two phases is a function of the contact length and the flow velocity. Another important parameter is the Laplace pressure ($\Delta P_{\mathrm{Laplace}}$) caused by the interfacial tension between two phases. The position of the interface is fixed within a point in the microchannel by the balance established between the $\Delta P_{\mathrm{Laplace}}$ and ΔP_{Flow}.

Figure 13a illustrates the pressure balance at the liquid–liquid interface of the two-phase microflows. The liquid–liquid interface curves toward the organic phase in a glass surface because of the hydrophilicity of the glass. $\Delta P_{\mathrm{Laplace}}$ is generated at the curved liquid–liquid

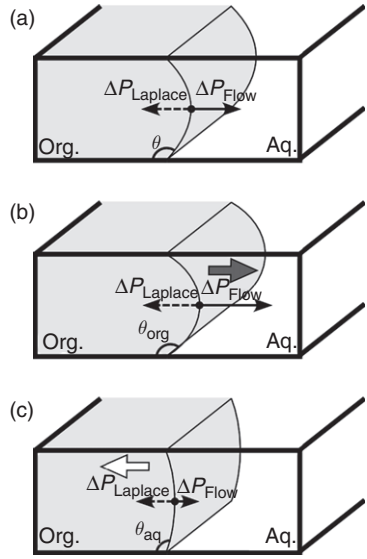

Figure 13 (a) Pressure balance at the liquid–liquid interface. Pressure difference is balanced with Laplace pressure when the two phases are separated. (b) When the pressure difference between the two phases is larger than the maximum Laplace pressure, the organic phase moves toward the aqueous phase. (c) When the pressure difference is lower than the minimum Laplace pressure, the aqueous phase moves toward the organic phase. Abbreviation: Aq., aqueous phase, Org., organic phase (Aota et al., 2009a).

interface. On the basis of the Young–Laplace equation, $\Delta P_{\text{Laplace}}$ is estimated as follows:

$$\Delta P_{\text{Laplace}} = \gamma\left(\frac{1}{R_1} + \frac{1}{R_2}\right) \tag{22}$$

where R_1 and R_2 are the curvature radii of the liquid–liquid interface in direction vertical and parallel to the liquid stream. For parallel multiphase microflows, the equation is simplified as follows:

$$\Delta P_{\text{Laplace}} = \gamma\left(\frac{1}{R_1}\right) = \frac{2\gamma \sin(\theta - 90°)}{d} \tag{23}$$

where θ and d are the contact angle and depth of the microchannels. The contact angle is restricted to the values between the advancing contact angle of the aqueous phase θ_{aq} and that of the organic phase θ_{org}. Therefore, $\Delta P_{\text{Laplace}}$ is restricted as follows:

$$\frac{2\gamma \sin(\theta_{\text{aq}} - 90°)}{d} < \Delta P_{\text{Laplace}} < \frac{2\gamma \sin(\theta_{\text{org}} - 90°)}{d} \tag{24}$$

When ΔP_{Flow} exceeds the maximum $\Delta P_{\text{Laplace}}$, the organic phase flows toward the aqueous phase (Figure 13b). When ΔP_{Flow} is lower than the minimum $\Delta P_{\text{Laplace}}$, the aqueous phase flows toward the organic phase (Figure 13c). When the flow rate ratio is changed, the pressure balance is maintained by changing the position of the liquid–liquid interface. This model indicates that the important parameters for microfluid control are the interfacial tension, the dynamic contact angle, and the depth of the microchannel. This model can also be applied to gas–liquid microflows.

Considering the interfacial pressure model, the flow rates should be between the higher and lower limits. ΔP_{Flow} can be evaluated by considering the pressure loss in the microchannels. Assuming that the pressure at the opened outlet is atmospheric pressure, P_{atm}, then the pressure P of each phase from the pressure loss ΔP is expressed as follows:

$$\begin{aligned} P &= P_{\text{atm}} + \Delta P_{\text{tube}} + \Delta P_{\text{channel}} \\ &= P_{\text{atm}} + \frac{2f\,\rho v_{\text{tube}}^2 L_{\text{tube}}}{d_{\text{h, tube}}} + \frac{2f\,\rho v_{\text{channel}}^2 L_{\text{channel}}}{d_{\text{h, channel}}} \end{aligned} \tag{25}$$

where f, ρ, v, and L are the friction factor, the density, the mean velocity of the fluid, and the length of the tube and channel. The subscripts of tube and channel correspond to the parts of the outlet tube and the microchannel. When the gas–liquid and liquid–liquid microflows are considered to be laminar flow, f is expressed as follows:

$$f = \frac{16}{\text{Re}} = \frac{16\mu}{\rho v d_{\text{h}}} \tag{26}$$

Therefore, ΔP_{Flow} can be expressed as follows:

$$\begin{aligned}\Delta P_{\mathrm{Flow}} &= P_{\mathrm{org}} - P_{\mathrm{aq}} \\ &= \frac{32\mu_{\mathrm{org}} v_{\mathrm{channel,org}} L_{\mathrm{channel,org}}}{{d_{\mathrm{h,\ channel,org}}}^2} + \frac{32\mu_{\mathrm{org}} v_{\mathrm{tube,org}} L_{\mathrm{tube,org}}}{{d_{\mathrm{h,\ tube,org}}}^2} \\ &\quad - \frac{32\mu_{\mathrm{aq}} v_{\mathrm{channel,aq}} L_{\mathrm{channel,aq}}}{{d_{\mathrm{h,\ channel,aq}}}^2} - \frac{32\mu_{\mathrm{org}} v_{\mathrm{tube,aq}} L_{\mathrm{tube,aq}}}{{d_{\mathrm{h,\ tube,aq}}}^2}\end{aligned} \tag{27}$$

where the subscripts org and aq correspond to the organic and aqueous phases, respectively. By utilizing Equation (27), the higher and lower limits of ΔP_{Flow} were evaluated. Table 2 summarizes the literature values of the viscosities of various solvents. $\Delta P_{\mathrm{Laplace}}$ can be evaluated by utilizing Equation (23). Table 3 summarizes the interfacial tension of various solvents. The advancing and receding contact angles of water on a glass

Table 2 Summary of viscosity of solvent at 20 °C

Solvent	Viscosity (cP)
Acetone	0.315
Aniline	4.40
1-Butanol	2.948
Butyl acetate	0.732
Carbon tetrachloride	0.969
Chloroform	0.58
Cyclohexane (at 17 °C)	1.02
1-Decanol	12.96
Dichloromethane	0.445
Diethyl ether (at 25 °C)	0.224
1,4-dioxane (at 25 °C)	1.177
Dodecane (at 25 °C)	1.383
Ethanol	1.20
Ethyl acetate	0.455
Hexane	0.326
Methanol	0.597
Nitrobenzene	2.03
1-Octanol (at 25 °C)	7.288
Pentane	0.240
1-Propanol	2.256
Toluene	0.590
Water	1.002
m-Xylene	0.620

Table 3 Summary of interfacial tension between air–solvent and aqueous–organic interfaces at 20 °C

Solvent	For air (mN m^{-1})	For water (mN m^{-1})
Acetone	25.3	
Aniline		6.1
1-Butanol		1.6
Butyl acetate		13.5
Carbon tetrachloride	27.6	
Chloroform	28.7	30.8
Cyclohexane		47.7
1-Decanol	28.6	
Dichloromethane	31.1	28.4
Diethyl ether	19.1	
1,4-Dioxane	34.2	
Dodecane	25.3	
Ethanol	22.7	
Ethyl acetate	24.3	6.3
Hexane	19.4	50.0
Methanol	23.5	
Nitrobenzene	43.3	25.2
1-Octanol	27.7	
Pentane	18.5	
1-Propanol	23.9	
Toluene	28.8	35.3
Water	72.0	
m-Xylene	28.7	36.6

plate in toluene are 10.2 $\pm$ 4.9° and 64.5 $\pm$ 4.3°, respectively. These values were also used for the contact angles in other organic solvents.

The phase separation conditions of liquid–liquid microflows for various organic solvents in the double-Y-type microchannel with a width of 215 μm, a depth of 34 μm, and a contact length of 20 mm are shown in Figure 14. The flow rate of the aqueous phase was fixed to be 10 μl min^{-1}. The experimental results agreed well with the theoretical values. The experimental results also agreed with simulated values obtained by the three-dimensional simulation using the volume of fluid method. Controlling ΔP_{Flow} and $\Delta P_{\mathrm{Laplce}}$ permits phase separation to be achieved in the microchannel. With the help of this, the researchers can design various microfluidic chemical processes using liquid–liquid microflows.

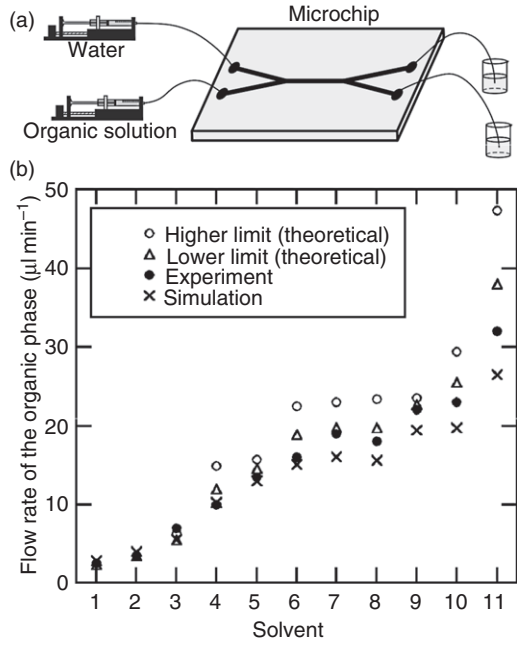

Figure 14 (a) Illustration of the microchip having a width of 215 μm, a depth of 35 μm, and a contact length of 20 mm. (b) Phase separation conditions of the liquid–liquid microflows. Solvents: 1, aniline; 2, 1-butanol; 3, nitrobenzene; 4, cyclohexane; 5, butyl acetate; 6, *m*-xylene; 7, chloroform; 8, toluene; 9, ethyl acetate; 10, dichloromethane; and 11, hexane. The opened circles show the theoretical higher limit, the opened triangles the theoretical lower limit, the solid circles experimental results, and the crosses the results of the simulation (Aota et al., 2009a).

The phase separation conditions of air–liquid microflows for various solvents in the double-Y-type microchannel with a width of 100 μm, a depth of 45 μm, and a contact length of 20 mm are shown in Figure 15. The flow rate of the air phase was fixed to be 1 ml min^{-1}. The results, however, did not agree with the theoretical values. Assuming only the pressure loss and the Laplace pressure, the phase separation should be achieved within the narrow range of the flow rates. However, phase separation was achieved over a wide range of flow rates. This disparity may be explained by considering the compression of the gas phase, evaporation of the liquid phase, and wetting at the outlet port of the liquid phase. Therefore, when gas–liquid microflows form in microchannels, the compressivity, vapor pressure, humidity, and pressure of the outlet should be carefully considered.

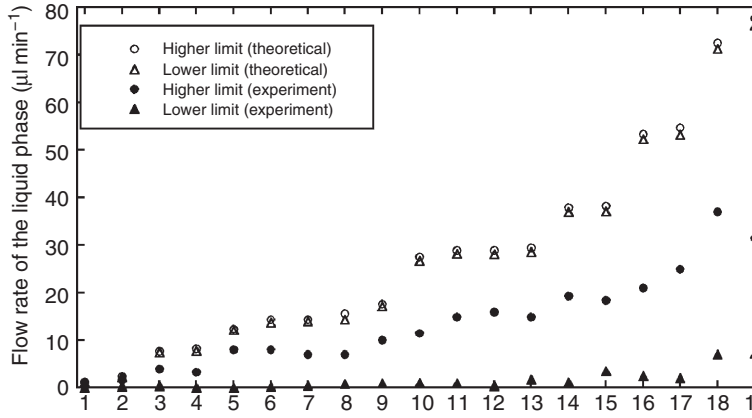

Figure 15 Phase separation conditions of the gas–liquid microflows. Solvents: 1, 1-decanol; 2, 1-octanol; 3, 1-propanol; 4, nitrobenzene; 5, dodecane; 6, 1,4-dioxane; 7, ethanol; 8, water; 9, carbon tetrachloride; 10, *m*-xylene; 11, hexane; 12, toluene; 13, chloroform; 14, ethyl acetate; 15, dichloromethane; 16, hexane; 17, acetone; 18, pentane; and 19, diethyl ether. The open circles show the theoretical higher limit, the open triangles the theoretical lower limit, the solid circles the experimental results of the higher limit, and the solid triangles the experimental results of the lower limit (Aota et al., 2009a).

3.2 Methods of stabilization of multiphase microflows

Disturbances in the flow rates of pumps can destabilize multiphase microflows. However, the control method utilizing the microchannel structure and surface energy is effective for maintaining robust control over microfluidics. Researchers have suggested that multiphase microflows can be stabilized by altering the structure or adding features to the microchannels, specifically by including a guide structure (Tokeshi et al., 2002) or a pillar structure (Maruyama et al., 2004) along the microchannel, which permit a wider range of contact angle for the fluid interface than a flat surface. Researchers can design various microfluidic chemical processes using liquid–liquid microflows.

Other groups have proposed selective chemical surface modification for stabilization of the multiphase microflows (Aota et al., 2007a, 2007b; Hibara et al., 2002, 2003, 2005, 2008; van der Linden et al., 2006; Zhao et al., 2001, 2002a, 2002b, 2003) Figure 16 illustrates the shape of the liquid–liquid interface in a microchannel with chemically patterned surfaces. The contact angle of water on a hydrophobic surface can be larger than 90°. Therefore, multiphase microflows in microchannels with patterned surfaces can form under a wider range of conditions compared to microchannels with a guide structure or pillar structure.

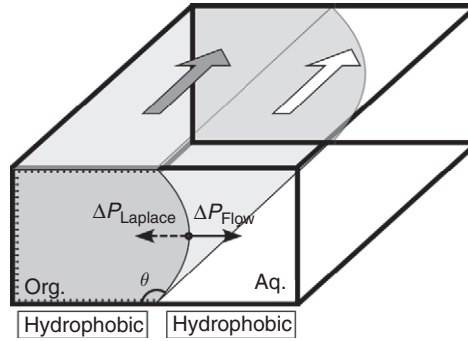

Figure 16 Shape of the liquid–liquid interface, whose contact line is pinned at the boundary between the hydrophilic and the hydrophobic surfaces.

Beebe's group has proposed a selective chemical surface modification method by combining multiphase laminar microflow and self-assembled monolayer (SAM) chemistry (Zhao et al., 2001, 2002a, 2002b, 2003). The flow in the microchannels is laminar flow as described in Section 3.1. Therefore, multiphase microflows of miscible solutions can flow side-by-side without turbulent mixing. A stream of pure hexadecane and a stream of octadecyltrichlorosilane (ODS) solution in hexadecane were introduced together in microchannels by syringe pumps, and laminar flow was maintained for 2–3 min (Figure 17). SAMs formed on both the top and bottom of the microchannels in the area containing the ODS solution. The other microchannels in the area without the ODS solution remain the hydrophilicity of the bare glass surface. The flow rates must be fast in order to prevent diffusion of ODS.

Beebe's group has also proposed a selective chemical surface modification method by photolithography (Zhao et al., 2001, 2002a, 2002b, 2003). This method uses photocleavable SAMs having hydrophobic and hydrophilic groups. First, the microchannels were modified using the photocleavable SAMs. The microchannels were cleaned by sequentially flushing

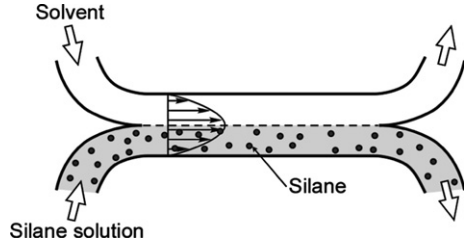

Figure 17 Schematic illustration of the selective surface modification using multiphase laminar microflows (Zhao et al., 2001).

with hexane and methanol after monolayer deposition from a 0.5 wt % solution of the corresponding trichlorosilane in hexadecane, and then dried with nitrogen. A photomask is placed on top of the SAM-modified microchannels filled with NaOH solution. Ultraviolet (UV) irradiation through a mask for 90 min leads to the production of hydrophilic groups in the irradiated regions (Figure 18).

Kitamori's group has proposed selective chemical surface modification utilizing capillarity (called the capillarity restricted modification or CARM method) (Hibara et al., 2005). In the CARM method, a microchannel structure combining shallow and deep microchannels and the principle of capillarity are utilized. The procedures are shown in Figure 19. A portion of an ODS/toluene solution (1 wt%) is dropped onto the inlet hole of the shallow channel, and the solution is spontaneously drawn into this channel by capillary action. The solution is stopped at the boundary between the shallow and deep channels by the balance between the solid–liquid and gas–liquid interfacial energies. Therefore, the solution does not enter the deep channel. It remains at the boundary for several minutes and is then pushed from the deep channel side by air pressure.

Since $\Delta P_{\mathrm{Laplace}}$ depends on the depth of the microchannels, more effective stabilization of multiphase microflows can be attained by utilizing shallow microchannels. For example, a microstructure combining shallow and deep microchannels with hydrophobic and hydrophilic surfaces, respectively, can yield large $\Delta P_{\mathrm{Laplace}}$. In a shallow 10-μm-deep microchannel, $\Delta P_{\mathrm{Laplace}}$ of the gas–water interface is 6 kPa. Microchannels with an asymmetric cross section with the patterned surfaces mentioned above are effective not only for the stability of the multiphase microflows, but also for a fail-safe system required for practical systems. Air bubbles contamination can disturb the stability of systems and liquid–liquid two-phase microflows sometimes are unstable due to some disturbances. By using microchannels having asymmetric cross sections along with the patterned surface, one can convert plug flow into two-phase microflows (Figure 20) (Hibara et al., 2005, 2008).

In chemically patterned microchannels, microcountercurrent flows can form (Aota et al., 2007a, 2007b, 2007c). In conventional macroscale devices, countercurrent flow is attained by gravitational segregation involving droplets (Figure 21a). However, parallel countercurrent flow in the laminar flow regime cannot be easily realized. In an ordinary microchannel, countercurrent flow cannot form because high shear stress at the interface causes breakup (Figure 21b) and the two phases collide (Figure 21c). To form parallel microcountercurrent flows, the aqueous solution must flow along one side of the channel and the organic solution must flow along the other side without breakup. Considering pressure balance at the interface, microcountercurrent flows can be formed in a microchannel with patterned surfaces. The phase separation conditions for gas–liquid and

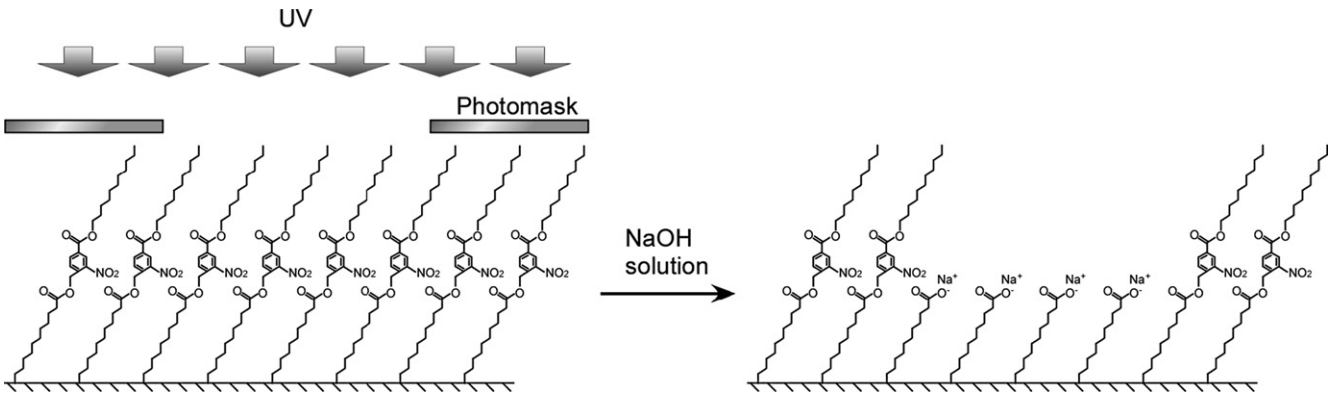

Figure 18 UV photopatterning method. The molecular structure of a photocleavable SAM formed on glass surfaces. UV irradiation through masks placed on top of SAM-modified microchannels leads to the production of hydrophilic carboxylate groups in the irradiated regions (Zhao et al., 2001).

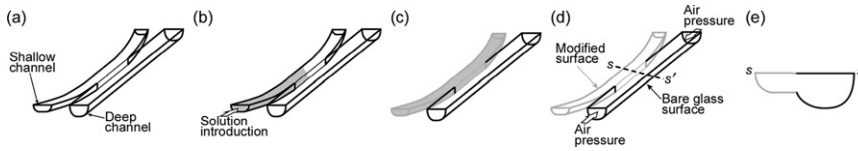

Figure 19 Modification procedures by CARM method. (a) The shallow and deep microchannels have separate inlet holes and contact points in the microchip. (b) A solution containing modification compounds is introduced from the inlet of the shallow microchannel by capillarity. (c) The solution does not leak to the deep microchannel and only the shallow microchannel is modified. (d) The solution is pushed away with air pressure from the deep microchannel. (e) A sectional illustration along the s–s′ dashed line in (d) (Hibara et al., 2005).

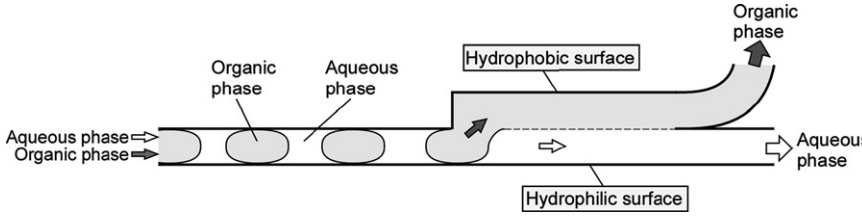

Figure 20 Conversion of plug flow into parallel two-phase microflows (Hibara et al., 2008).

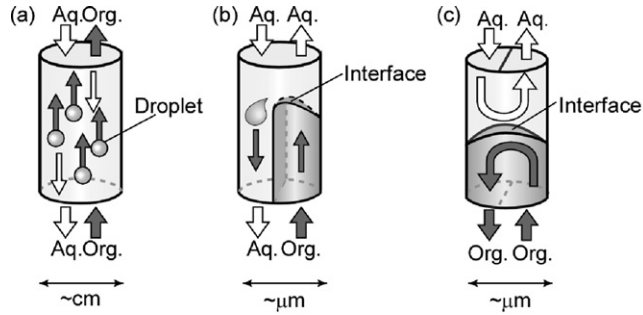

Figure 21 Schematic illustration of (a) countercurrent flows in conventional macroscale devices, (b) droplet generation because of breakup due to high shear stress in an ordinary microchannel, and (c) collision of two phases in an ordinary microchannel. Abbreviation: Aq., aqueous phase, Org., organic phase (Aota et al., 2007c).

liquid–liquid microcountercurrent flows in the microchannel with an asymmetric cross section are shown in Figure 22. Since the viscosity of air can be thought of as being negligible, the maximum flow rate of water becomes constant under experimental conditions. The theoretical higher limit value is shown as the solid line in Figure 22b. Experimental results

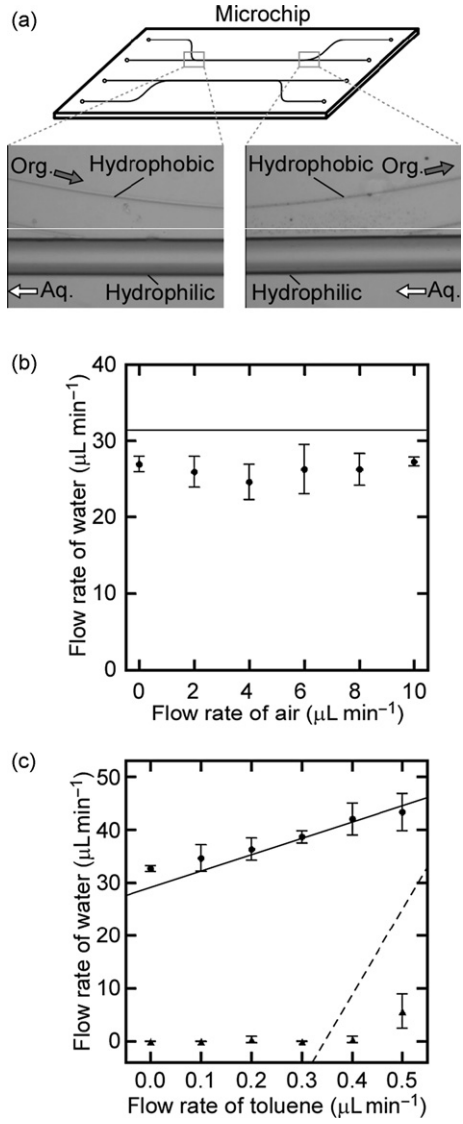

Figure 22 (a) Optical microscope images of the phase separation at the confluences. (b) Maximum flow rate of water as a function of the flow rate of air. The solid circles show the experimental maximum flow rates and the solid line theoretical higher limit. (c) Maximum and flow rates of water as a function of the flow rate of toluene. The solid circles show the experimental maximum flow rates, the solid triangles the experimental minimum flow rates, the solid line theoretical higher limit, and the dashed line the theoretical lower limit (Aota et al., 2007a).

differed slightly from the theoretical value, a discrepancy that could be explained by experimental issues around the outlet of the microchannel, such as pressure loss and wetting. Considering the theoretical lower limit, the viscosity of air of 18.6 μPa s at 300 K is only 1.9% that of water. Therefore, the pressure of the air phase can be considered to be negligible. Figure 22c shows the phase separation conditions of the aqueous toluene microcountercurrent flows. For liquid–liquid microcountercurrent flows, the viscosities of both phases play an important role. Therefore, the higher and lower limits are not constant. The theoretical higher and lower limit values are shown as the solid and dashed lines in Figure 22c, respectively. The maximum flow rate in the upstream part of the aqueous phase agreed well with the theoretical value. The minimum flow rate, however, did not agree with the theoretical values. This disparity could be explained in terms of the microchannel geometry. When water leaks onto the hydrophobic surface, the contact angle on the upper wall is the same as that on the lower wall because the hydrophobic channel is flat. However, when toluene leaks onto the hydrophilic surface, the contact angle on the upper wall is different from that on the lower wall because the hydrophilic channels has a semicircular cross section and the boundary between the hydrophilic and hydrophobic surfaces has an edge. Since the range of contact angles of the liquid–liquid interface at the edge becomes wider compared to that on a flat surface, the liquid–liquid interface at the edge structure can produce a larger value of $\Delta P_{\mathrm{Laplace}}$ than from a flat surface. Since the edge structure can expand the range of flow rate conditions for phase separation, this disagreement may not be a serious problem for the design of microfluidic chemical processes utilizing multiphase microflows.

Gas–liquid and liquid–liquid microflows are effective for highly efficient extraction processes. When samples comprise adsorbent molecules at a fluid–liquid interface, molecular adsorption changes the interfacial tension of the fluid–liquid interface. Since the specific interfacial area is very large in a microchip, the change in interfacial tension due to molecular adsorption can be an important factor affecting phase separation of the gas–liquid and liquid–liquid microflows. The molecular concentration is higher in the downstream portion of the microflows. Thus, when designing a chemical process that includes molecular transport through the interface, researchers need to modify the proposed model by considering molecular adsorption at the interface. For microextraction design, the *in situ* interfacial tension measurement is especially important. The microscopic quasielastic laser scattering method could be a powerful tool for this purpose (Hibara et al., 2003).

Superhydrophilic and superhydrophobic surfaces are more effective at stabilizing two-phase microflows. These surfaces can be obtained by creating roughness utilizing titanium nanoparticles. Titanium modification of a microchannel yields nanometer-scale surface roughness, and subsequent

hydrophobic treatment creates a superhydrophobic surface. Photocatalytic decomposition of the coated hydrophobic molecules was used to pattern the surface wettability, which was tuned from superhydrophobic to superhydrophilic under controlled photoirradiation (Takei et al., 2007a). This method can also be applied to the conversion of plug flow into two-phase microflows.

3.3 Wettability-based microvalve

Numerous miniaturized mechanical valves fabricated by micromachining technologies have been developed (Auroux et al., 2002; Dittrich et al., 2006; Reyes et al., 2002). Pneumatic-controlled valves made of soft material have also been reported (Unger et al., 2000). All of these valves require both fabrication and construction of mechanical moving parts or the pressure of external control parts in the microchannels. Also, there have been reports of nonmechanical methods utilizing phase transition solution (Gui and Liu, 2004), a thermoresponsive polymer (Yu et al., 2003), or hydrogel (Beebe et al., 2000). Additionally, patterned hydrophobic surfaces have been demonstrated as valves for microfluid control in a variety of applications. The patterned titanium surfaces described previously can be used very effectively as valves in a microchip due to their superhydrophobic nature (Takei et al., 2007b). Batch operation in the microchannels with patterned surfaces has been demonstrated as shown in Figure 23. First, fluorescent solution was introduced at a pressure below the maximum Laplace pressure (Figure 23a). Second, air was introduced at the same pressure to push out excess solution and retain the plug of picoliter volume (Figure 23b). Third, air was introduced at a pressure

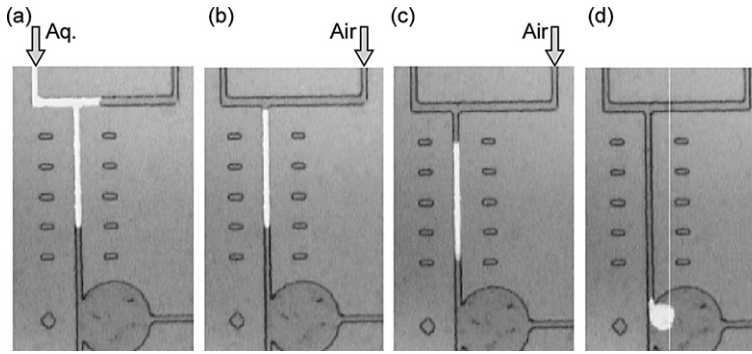

Figure 23 Fluorescence images of the liquid motion during batch operation in a microchannel. The liquid is (a) being introduced, (b) measured, (c) transferred, and (d) dispensed to the other channel (Takei et al., 2007b).

higher than the maximum Laplace pressure to expel the plug (Figure 23c, d). This microvalve-utilizing chemical surface modification has no dead volume and can supply a constant volume of liquid for reaction or analysis. Moreover, the repeatability of this operation allows it to be applied to titration.

4. DISCUSSION AND CONCLUSIONS

The basic methodologies and applications for microfluidics were introduced. In Chapter 2, the general concepts (MUO and CFCP) for microintegration and applications based on CFCP will be discussed. CFCP approach can be applied to develop more complicated chemical processing system. If CAD for microchemical processing, which includes microfluid simulation, reaction time analysis, extraction time analysis, and microchennel structure design, the time of development for microchemical systems would be drastically shortened. In Chapter 3, fluid control methods will be discussed. The viscous force and the interfacial tension are effective forces in microspaces. In order to control these forces, surface chemistry and microchannel structures play important roles. Since the basic methodologies have already been developed, development of microfluidic systems for practical applications is required in the next stage.

LIST OF SYMBOLS

a	width of phase I (m)
b	width of phase II (m)
d	depth (m)
d_h	equivalent diameter (m)
f	friction factor (-)
g	gravitational acceleration ($m\,s^{-2}$)
K	diffusion coefficient ($m^2\,s^{-1}$)
L	channel length (m)
l_p	perimeter (m)
l_d	diffusion length (m)
P	pressure ($N\,m^{-2}$)
P_{atm}	atmospheric pressure ($N\,m^{-2}$)
R	curvature radius (m)
S	cross section (m^2)
t	diffusion time (s)
u	mean velocity ($m\,s^{-1}$)

v	flow velocity (m/s)
w	width (m)

GREEK LETTERS

γ	interfacial tension ($N\,m^{-1}$)
μ	viscosity (cP)
ΔP	pressure difference ($N\,m^{-2}$)
ΔP_{Flow}	pressure difference between two phases ($N\,m^{-2}$)
ΔP_{Laplce}	Laplace pressure ($N\,m^{-2}$)
$\Delta\rho$	density difference ($kg\,m^{-3}$)
θ	contact angle (degree)
θ_{aq}	advancing contact angle of aqueous phase (degree)
θ_{org}	advancing contact angle of organic phase (degree)
ρ	density ($kg\,m^{-3}$)
τ	shear stress ($N\,m^{-2}$)

REFERENCES

Aota, A., Hibara, A., and Kitamori, T. *Anal. Chem.* **79**, 3919–3924 (2007a).

Aota, A., Hibara, A., and Shinohara, K., et al. *Anal. Sci.* **23**, 131–133 (2007b).

Aota, A., Mawatari, K., and Takahashi, S., et al. *Microchim. Acta* **164**, 249–255 (2009a).

Aota, A., Mawatari, K., and Kihira, Y., et al. Micro continuous gas analysis system of ammonia in cleanroom, *in* "Proceedings of Micro Total Analysis Systems 2009" (T. Kim, Y. S. Lee, T. D. Chung, N. L. Jeon, S. H. Lee, K. Y. Suh, J. Choo, Y. K. Kim Eds.), pp. 609–611. The Chemical and Biological Microsystems Society, Jeju-island, Korea (2009b).

Aota, A., Nonaka, M., and Hibara, A., et al. *Angew. Chem. Int. Ed.* **46**, 878–880 (2007c).

Auroux, P. A., Lossifidis, D., and Reyes, D. R., et al. *Anal. Chem.* **74**, 2637–2652 (2002).

Beebe, D. J., Moore, J. S., and Bauer, J. M., et al. *Nature* **404**, 588–590 (2000).

Brody, J. P., and Yager, P. *Sens. Actuators, A* **58**, 13–18 (1997).

Burns, J. R., and Ramshaw, C. *Lab Chip* **1**, 10–15 (2001).

Dittrich, P. S., Tachikawa, K., and Manz, A. *Anal. Chem.* **78**, 3887–3908 (2006).

Goto, M., Sato, K., and Murakami, A., et al. *Anal. Chem.* **77**, 2125–2131 (2005).

Goto, M., Tsukahara, T., and Sato, K., et al. *Anal. Bioanal. Chem.* **390**, 817–823 (2008).

Gui, L., and Liu, J. *J. Micromech. Microeng.* **14**, 242–246, (2004).

Hachiya, H., Matsumoto, T., and Kanda, K., et al., Micro environmental gas analysis system by using gas-liquid two phase flow, *in* "Proceedings of Micro Total Analysis Systems 2004" (T. Laurell, J. Nillson, K. F. Jensen, D. J. Harrison, J. P. Kutter Eds.), pp. 91–101. Royal Society of Chemistry, Mölme, Sweden (2004).

Hibara, A., Iwayama, S., and Matsuoka, S., et al. *Anal. Chem.* **77**, 943–947 (2005).

Hibara, A., Kasai, K., and Miyaguchi, H., et al. Novel two-phase flow control concept and multi-step extraction microchip, *in* "Proceedings of Micro Total Analysis Systems 2008" (L. E. Locascio, M. Gaitan, B. M. Paegel, D. J. Ross, W. N. Vreeland Eds.), pp. 1326–1328. Chemical and Biological Microsystems Society, San Diego, USA, (2008).

Hibara, A., Nonaka, M., and Hisamoto, H., et al. *Anal. Chem.* **74**, 1724–1728 (2002).

Hibara, A., Nonaka, M., and Tokeshi, M., et al. *J. Am. Chem. Soc.* **125**, 14954–14955 (2003).
Hibara, A., Tokeshi, M., and Uchiyama, K., et al. *Anal. Sci.* **17**, 89–93 (2001).
Hiki, S., Mawatari, K., and Hibara, A., et al. *Anal. Chem.* **78**, 2859–2863 (2006).
Hisamoto, H., Horiuchi, T., and Tokeshi, M., et al. *Anal. Chem.* **73**, 1382–1386 (2001a).
Hisamoto, H., Horiuchi, T., and Uchiyama, K., et al. *Anal. Chem.* **73**, 5551–5556 (2001b).
Hisamoto, H., Shimizu, Y., and Uchiyama, K., et al. *Anal. Chem.* **75**, 350–354 (2003).
Hotokezaka, H., Tokeshi, M., and Harada, M., et al. *Prog. Nucl. Energy* **47**, 439–447 (2005).
Kakuta, M., Takahashi, H., and Kazuno, S., et al. *Meas. Sci. Technol.* **17**, 3189–3194 (2006).
Kikutani, Y., Hisamoto, H., and Tokeshi, M., et al. *Lab Chip* **4**, 328–332 (2004).
Kopp, M. U., de Mello, A. J., and Manz, A. *Science* **280**, 1046–1048 (1998).
Kralj, J. G., Schmidt, M. A., and Jensen, K. F. *Lab Chip* **5**, 531–535, (2005).
Maruyama, T., Kaji, T., and Ohkawa, T., et al. *Analyst* **129**, 1008–1013 (2004).
Mawatari, K., Tokeshi, M., and Kitamori, T. *Anal. Sci.* **22**, 781–784 (2006).
Minagawa, T., Tokeshi, M., and Kitamori, T. *Lab Chip* **1**, 72–75 (2001).
Miyaguchi, H., Tokeshi, M., and Kikutani, Y., et al. *J. Chromatogr. A* **1129**, 105–110 (2006).
Ohashi, T., Mawatari, K., Sato, K., et al. Automated micro-ELISA system for allergy checker: a prototype and clinical test, *in* "Proceedings of Micro Total Analysis Systems 2006" (T. Kitamori, H. Fujita, S. Hasebe Eds.), pp. 858–860. Japan Academic Association Inc., Japan (2006).
Proskurnin, M. A., Slyadnev, M. N., and Tokeshi, M., et al. *Anal. Chim. Acta* **480**, 79–95 (2003).
Reyes, D. R., Lossifidis, D., and Auroux, P. A., et al. *Anal. Chem.* **74**, 2623–2636 (2002).
Sahoo, H. R., Kralj, J. G., and Jensen, K. F. *Angew. Chem. Int. Ed.* **46**, 5704–5708 (2007).
Sato, K., Tokeshi, M., and Kimura, H., et al. *Anal. Chem.* **73**, 1213–1218 (2001).
Sato, K., Tokeshi, M., and Kitamori, T., et al. *Anal. Sci.* **15**, 641–645 (1999).
Sato, K., Tokeshi, M., and Odake, T., et al. *Anal. Chem.* **72**, 1144–1147 (2000a).
Sato, K., Tokeshi, M., and Sawada, T., et al. *Anal. Sci.* **16**, 455–456 (2000b).
Sato, K., Yamanaka, M., and Hagino, T., et al. *Lab Chip* **4**, 570–575 (2004).
Sato, K., Yamanaka, M., and Takahashi, H., et al. *Electrophoresis* **23**, 734–739 (2003).
Slyadnev, M. N., Tanaka, Y., and Tokeshi, M., et al. *Anal. Chem.* **73**, 4037–4044 (2001).
Smirnova, A., Mawatari, K., and Hibara, A., et al. *Anal. Chim. Acta* **558**, 69–74, (2006).
Smirnova, A., Shimura, K., and Hibara, A., et al. *Anal. Sci.* **23**, 103–107 (2007).
Song, H., Tice, J. D., and Ismgailov, R. F. *Angew. Chem. Int. Ed.* **42**, 767–772 (2003).
Sorouraddin, H. M., Hibara, A., and Kitamori, T. *Fresenius' J. Anal. Chem.* **371**, 91–96 (2001).
Sorouraddin, H. M., Hibara, A., and Proskrunin, M. A., et al. *Anal. Sci.* **16**, 1033–1037 (2000).
Surmeian, M., Hibara, A., and Slyadnev, M., et al. *Anal. Lett.* **34**, 1421–1429, (2001).
Surmeian, M., Sladnev, M. N., and Hisamoto, H., et al. *Anal. Chem.* **74**, 2014–2020 (2002).
Takei, G., Aota, A., and Hibara, A., et al. Phase separation of segmented flow by the photocatalytic wettability patterning and tuning of microchannel surface, *in* "Proceedings of Micro Total Analysis Systems 2007" (J. L. Viovy, P. Tabeling, S. Descroix, L. Malaquin Eds.), pp. 1213–1215. The Chemical and Biological Microsystems Society, Paris, France (2007a).
Takei, G., Nonogi, M., and Hibara, A., et al. *Lab Chip* **7**, 596–602 (2007b).
Tamaki, E., Hibara, A., and Tokeshi, M., et al. *J. Chromatogr. A* **987**, 197–204 (2003).
Tamaki, E., Hibara, A., and Tokeshi, M., et al. *Lab Chip* **5**, 129–131 (2005).
Tamaki, E., Sato, K., and Tokeshi, M., et al. *Anal. Chem.* **74**, 1560–1564 (2002).
Tanaka, Y., Sato, K., and Yamato, M., et al. *Anal. Sci.* **20**, 411–423 (2004).
Tanaka, Y., Sato, K., and Yamato, M., et al. *J. Chromatogr. A* **1111**, 233–237 (2006).
Tanaka, Y., Slyadnev, M. N., and Hibara, A., et al. *J. Chromatogr. A* **894**, 45–51 (2000).
Tokeshi, M., Minagawa, T., and Kitamori, T. *Anal. Chem.* **72**, 1711–1714 (2000a).
Tokeshi, M., Minagawa, T., and Kitamori, T. *J. Chromatogr. A* **894**, 19–23 (2000b).
Tokeshi, M., Minagawa, T., and Uchiyama, K., et al. *Anal. Chem.* **74**, 1565–1571, (2002).
Tokeshi, M., Uchida, M., and Hibara, A., et al. *Anal. Chem.* **73**, 2112–2116 (2001).

Tokeshi, M., Yamaguchi, J., and Hattori, A., et al. *Anal. Chem.* **77**, 626–630 (2005).
Unger, M. A., Chou, H. P., and Thorsen, T., et al. *Science* **288**, 113–116 (2000).
van der Linden, H. J., Jellema, L. C., and Holwerda, M., et al. *Anal. Bioanal. Chem.* **385**, 1376–1383 (2006).
Weigl, B. H., and Yager, P. *Science* **283**, 346–347 (1999).
Yamauchi, M., Mawatari, K., and Hibara, A., et al. *Anal. Chem.* **78**, 2646–2650 (2006).
Yu, C., Mutlu, S., Selvaganapathy, P., and Mastrangelo, C. H., et al. *Anal. Chem.* **75**, 1958–1961 (2003).
Zhao, B., Moore, J. S., and Beebe, D. J. *Science* **291**, 1023–1026 (2001).
Zhao, B., Moore, J. S., and Beebe, D. J. *Anal. Chem.* **74**, 4259–4268 (2002a).
Zhao, B., Moore, J. S., and Beebe, D. J. *Langmuir* **19**, 1873–1879 (2003).
Zhao, B., Viernes, N. O.L., and Moore, J. S., et al. *J. Am. Chem. Soc.* **124**, 5284–5285 (2002b).